Available online at www.sciencedirect.com
ScienceDirect
International Journal of Heat and Mass Transfer 51 (2008) 3387–3398
International Journal of HEAT and MASS TRANSFER
www.elsevier.com/locate/ijhmt

Mathematical formulation and numerical modeling of wax deposition in pipelines from enthalpy–porosity approach and irreversible thermodynamics

R. Banki [a,1], H. Hoteit [b,2], A. Firoozabadi [b,c,*]

[a] Imperial College, London, United Kingdom
[b] Reservoir Engineering Research Institute (RERI), Palo Alto, CA, USA
[c] Yale University, New Haven, CT, USA

Received 6 July 2007; received in revised form 1 November 2007
Available online 7 February 2008

Abstract

In the last 10 years, there have been a number of studies in modeling of the deposition processes in flowlines. Most of these models: (1) assume empirical or semi-empirical correlations to predict the pressure drop and temperature profile, (2) ignore the radial convection flow in the layer composed of the two-phase wax and oil (that is the gel layer), and (3) use Fick's law to describe the diffusion flux of species towards the wall by using the chain rule to relate concentration gradient to temperature gradient. In this work, a rigorous mathematical model for the prediction of wax deposition in pipelines is presented for laminar flow. The transient deposition of each component is calculated from the solution of the coupled momentum, energy and, species balance equations, and a thermodynamic wax precipitation model at the local level. An enthalpy formulation based on a fixed-grid approach is used to approximate the convection flow in the gel layer. We do not use the chain rule to relate composition gradient to temperature gradient in Fick's law to avoid violating the laws of irreversible thermodynamics. Our diffusion flux expression includes molecular diffusion (concentration gradient is driving force) and thermal diffusion (temperature gradient is driving force) with appropriate diffusion coefficients. This work also includes the description of the numerical solution of the governing equations. Numerical results and features of wax deposition as well as model verification with experimental data are presented in a separate paper.

Keywords: Wax deposition; Multicomponent diffusion; Wax hardening and aging

1. Introduction

Solid deposition from liquids in both natural and industrial processes can be undesirable and may result in harm. Examples of solid precipitation include frost formation on cold surfaces, crystallization fouling in heat exchangers, and wax and scale formation in flowlines in petroleum production.

As the search for oil and gas moves towards deeper waters such as the Gulf of Mexico and in the North Sea, the deposition of wax crystals in oil and gas pipelines becomes a major concern. The deposition in production tubings and pipelines is undesirable because of decrease in the flow rate and other operational complexities. To prevent blockage of pipelines, wax deposits should be removed periodically. Different mechanical, thermal, and chemical techniques can be used for wax removal [1–5].

Petroleum fluids are composed of a diverse group of species. The paraffinic groups with carbon numbers of say 15

* Corresponding author. Address: 385 Sherman Avenue, Suite 5, Palo Alto, CA 94306, USA. Tel.: +1 650 326 9172.
E-mail address: abbas.firoozabadi@yale.edu (A. Firoozabadi).
[1] Now with Halliburton, 2107 CityWest Blvd., Building 2, Houston, TX 77042, United States.
[2] Now with Conocophillips, 600 North Dairy Ashford (77079-1175), Houston, TX 77252, United States.

0017-9310/$ - see front matter © 2007 Published by Elsevier Ltd.
doi:10.1016/j.ijheatmasstransfer.2007.11.012

Nomenclature

Greek symbols

$\delta_{ik} = \delta_{ki}$	interaction parameter between component i and k
ε	porosity
μ	viscosity, Pa s
ρ	density, kg/m^3
τ	viscous stress
λ_i	molar latent heat of solidification of component

Alphabet symbols

A	momentum equation source term coefficient
a	PR-EOS parameter $= \sum_{i=1}^{n}\sum_{k=1}^{n} x_i x_k a_{ik}$
a_{ik}	PR-EOS parameter $= (1-\delta_{ik}) a_i^{1/2} a_k^{1/2}$
a_i	PR-EOS parameter $= 0.45724 R^2 T_{ci}^2 / P_{ci}$
b	PR-EOS parameter $= \sum_{i=1}^{n} x_i b_i$
b_i	PR-EOS parameter $= 0.07780 R T_{ci} / P_{ci}$
c	total molar density, mol/m^3
c_j	molar density of phase j, mol/m^3
c_{ji}	molar density of component i in phase j, mol/m^3
Cp_{ji}	heat capacity per unit mole of component i in phase$j$, J/mol K
Cp_j	heat capacity of per unit mole of phase j, J/mol K
ΔCp_i	difference in heat capacity of component i in liquid and solid state, J/mol K
$D^{\mathrm{M}}_{j,i,k}$	molecular diffusion coefficient in phase j, m^2/s
$\boldsymbol{D}^{\mathrm{M}}$	molecular diffusion coefficient matrix
$\boldsymbol{D}^{\mathrm{M}}_j$	molecular diffusion coefficient matrix of phase j
D^{T}_{ji}	thermal diffusion coefficient in phase j, m^2/K s
$\boldsymbol{D}^{\mathrm{T}}$	thermal diffusion coefficient vector
$\boldsymbol{D}^{\mathrm{T}}_j$	thermal diffusion coefficient vector of phase j
e	multicomponent energy flux, J/m^2 s
F	feed mole number, mol
f_i	fugacity of component i, Pa
H_j	molar enthalpy of component i in phase j, J/mol
H^*	ideal gas molar enthalpy of mixture at zero pressure, J/mol
H^*_i	ideal gas molar enthalpy of component I at zero pressure, J/mol
Δh^{f}_i	molar enthalpy of fusion of component I, J/mol
$(\boldsymbol{J}_{j,i})_r$	radial diffusion of component i, mol/m^2 s
$\boldsymbol{J}_{j,i}$	diffusion flux of component i in phase j, mol/m^2 s
$\boldsymbol{J}_j$	diffusion flux vector in phase j
$\boldsymbol{J}$	total diffusion flux vector
K	permeability, m^2
k	thermal conductivity, W/m K
L	pipe length, m
n	total number of components
n_{s}	number of solid phases
p	pressure, Pa
P_{ci}	critical pressure of component i, Pa
P^{f}_i	melting point pressure of component i, Pa
p_0	outlet pressure, Pa
Q	inlet volumetric flow rate, m^3/h
$\boldsymbol{q}$	energy flux relative to the mass–average velocity, W/m^2
$q^{(x)}$	Dufour effect, W/m^2
R	radial distance from pipe center, m
R	gas constant, J/mol K
R_0	pipe radius, m
Re	Reynolds number
S	source term
S_j	saturation of phase j
T	time, s
T	temperature, K
T_{a}	ambient temperature, K
T_{ci}	critical temperature of component i, K
T_{in}	inlet temperature, K
$\boldsymbol{v}$	velocity, m/s
$\boldsymbol{v}_{ji}$	velocity of component i in phase j, m/s
v_r	radial velocity, m/s
v_z	axial velocity, m/s
x_{ji}	molar composition of component i in phase j
Z	compressibility factor
z_i	overall composition of component i

to some 60 have high crystallization temperatures and may crystallize even at low concentration in the petroleum fluid mixture. The crystallites from petroleum fluids are often referred to as waxes; the temperature at which crystallization occurs is referred to as wax-appearance temperature (WAT).

An understanding of the mechanisms of the wax deposition and modeling of the process is likely to be a key step towards an optimum design and prevention of the problem.

There has been an extensive effort in the last decade to develop theoretical models for wax deposition calculations. In recent years, there has been success in the prediction of wax precipitation from crude oils and gas condensate fluids for local equilibrium calculations [6]. However, despite much progress, the more complicated problem of wax deposition in non-isothermal flowlines is still in an early stage of development.

There are two main processes that affect the deposition of wax in flowlines: (1) heat transfer, and (2) species flow. The heat transfer is mainly from conduction and convection. The flux of species by convection and diffusion is expected to strongly influence the deposition. To the best of our knowledge, the radial convective velocity in the region containing the deposition for the laminar flow has been neglected in the past [7–16]. The radial velocity is

expected to be small in comparison to axial velocity, but its contribution to species flux in the radial direction may be comparable to radial diffusion flux (due to non-uniform wax deposition, radial convection develops). One objective of this work is to include the radial convective flux in the formulation.

Wax deposition is a moving boundary problem and the numerical solution of the balance equations can be a challenge. A large number of numerical techniques are available for the solution of a moving boundary problem. There are two main approaches. In the transformed-grid approach, the governing differential equations and their boundary conditions are cast into a generalized curvilinear coordinate system. The equations can then be solved on a uniform-rectangular grid, which remains fixed in space and time. In essence, the moving boundary is immobilized. Extra terms in balance equations may be required for conservation of mass, momentum, and energy [17]. In the fixed-grid approach, which is also known as the enthalpy–porosity approach [18], a fixed grid is applied directly in real space (that is, the problem domain) and the interface conditions are accounted for by the definition of suitable source terms in the governing equations [18–20].

The enthalpy–porosity approach has been successfully implemented in many engineering problems that involve a liquid to solid phase change such as freezing of a pure liquid in a thermal cavity and melting of a pure metal [18,21,22]. In this work, we adopt this approach for the first time in the formulation of wax deposition by treating the layer with deposition as a pseudo-porous medium. Various authors have shown that the crystallization of paraffins in oil leads to the formation of gel with a complex morphology. The gelation is due to flocuulation of orthorhombic wax crystallites that appear in the solution. Observation with cross-polarized microscopy has revealed that the crystallites have structures of platelets that overlap and interlock and a network structure of wax crystals are formed [15,23,24]. Therefore, the gel behaves as porous media. In this work the Darcy-type source term is added to the momentum equation to describe the deceleration of flow in the gel layer. The energy equation for the multicomponent, two-phase flow is written in terms of the enthalpy. The relationship between the enthalpy and the temperature can be described by an equation of state.

To the best of our knowledge, in all the models in the literature the driving force for radial diffusion is first written in terms of concentration gradient and then through the chain rule, the temperature gradient is introduced [7–11,13–16,25,26]. In other words, various authors use the molecular diffusion coefficients with the driving force represented by temperature gradient. Thermodynamics of irreversible processes offers a different representation of diffusion with temperature gradient. In our formulation, we represent the molecular diffusion (driving force is concentration gradient), and thermal diffusion (driving force is temperature gradient) from thermodynamics of irreversible processes. Proper representation of diffusion fluxes and the study of diffusion effects are major goals of this work.

This paper is organized as follows. First, a detailed description of the mathematical model is presented for the coupled momentum, energy, and mass balances. We then provide the thermodynamics of wax-precipitation model followed by presenting the numerical formulation of the governing equations and the algorithm. The work is ended with a general summary and concluding remarks emphasizing that concentration gradient and temperature gradient may not be related through a chain rule.

2. Domain definition and basic assumptions

We consider a horizontal pipe of length L and inner radius R_0 (Fig. 1). A multicomponent fluid is injected at one end with a volumetric flow rate Q at temperature, T_{in}. The pipe wall temperature is set at constant temperature, T_a where $T_a < T_{in}$. The outlet pressure is held constant at p_0. We assume single-phase and gel subdomains as shown in Fig. 1. The formation of solid wax crystals creates a gel layer, which consists of a liquid phase and a nonmoving solid phase [15]. Studies of distillate fuels and model petroleum fluids reveal that as little as 2% of the crystal precipitate is required to gel the fluid [15,23,24,27]. When the amount of crystallites increases, the gel hardens. The process is called aging of the gel layer. The following assumptions are made in our work:

(1) Shear dispersion and Brownian diffusion are neglected.
(2) Gravity is neglected.
(3) Diffusions (both thermal and molecular) are neglected in the axial direction.
(4) Diffusion is neglected in the solid phase.
(5) Solid heat capacity and fluid thermal conductivity of each component are assumed temperature independent.
(6) Laminar flow is assumed.
(7) Multisolid wax precipitation is assumed.

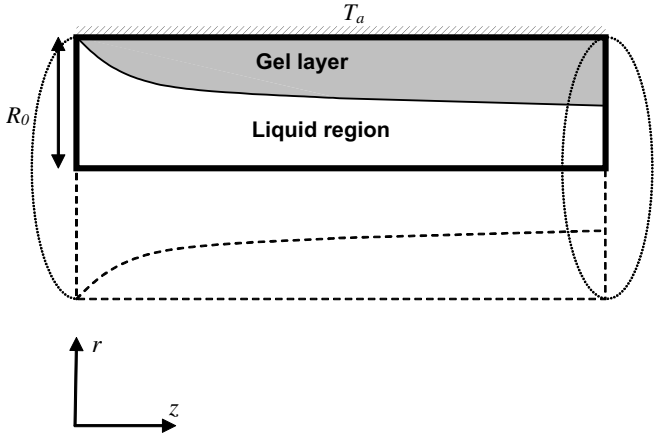

Fig. 1. Computational domain, the geometry of problem is a 2D circular coordinate system.

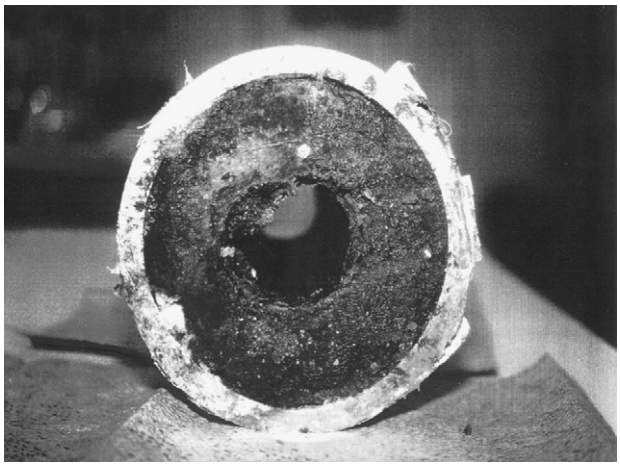

Fig. 2. Wax deposition in a subsea pipeline, a schematic view on how severely wax deposits can obstruct the pipeline.

By neglecting the gravity effect, the 3D computational problem is reduced to 2D (see Fig. 1). There is ample evidence, based on the examination of the deposition in pipelines, that this is a good assumption. Fig. 2 shows one example of wax deposition in subsea pipeline where the whole line had to be abandoned due to a hardened nature of wax deposits.

3. Mathematical model

Below the wax appearance temperature (WAT), part of heavy components may precipitate and form a gel layer next to the pipe wall. The gel layer consists of liquid and immobile solid wax. The hardening of the gel layer is mainly by convection and diffusion and the subsequent increase in the fraction of deposited wax. The temperature, pressure, velocity field, and composition are related through:

(1) Momentum balance.
(2) Energy balance.
(3) Species balance.
(4) Local solid/liquid equilibrium.

3.1. Momentum balance

In cylindrical coordinates, the momentum equation is given in the z- and r-directions for a compressible single-phase liquid flow by the following expressions [28,29]:

$$\left[\frac{\partial(\rho v_z)}{\partial t}+\frac{1}{r}\frac{\partial(r\rho v_r v_z)}{\partial r}+\frac{\partial(\rho v_z v_z)}{\partial z}\right] = -\frac{\partial p}{\partial z}+\left[\frac{1}{r}\frac{\partial}{\partial r}(r\tau_{rz})+\frac{\partial \tau_{zz}}{\partial z}\right], \quad (1)$$

$$\left[\frac{\partial(\rho v_r)}{\partial t}+\frac{1}{r}\frac{\partial(r\rho v_r v_r)}{\partial r}+\frac{\partial(\rho v_z v_r)}{\partial z}\right] = -\frac{\partial p}{\partial r}+\left[\frac{1}{r}\frac{\partial}{\partial r}(r\tau_{rr})-\frac{\tau_{\theta\theta}}{r}+\frac{\partial \tau_{zr}}{\partial z}\right]. \quad (2)$$

We use v_z and v_r to denote the velocity components in the liquid phase in the z- and r-directions, respectively. In the two equations above, the stress terms are given by

$$\tau_{zz}=2\mu\left[\frac{\partial v_z}{\partial z}-\frac{1}{3}\nabla.\boldsymbol{v}\right], \quad \tau_{rr}=2\mu\left[\frac{\partial v_r}{\partial r}-\frac{1}{3}\nabla\cdot\boldsymbol{v}\right],$$
$$\tau_{\theta\theta}=2\mu\left[\frac{v_r}{r}-\frac{1}{3}\nabla\cdot\boldsymbol{v}\right], \quad \tau_{rz}=\tau_{zr}=\mu\left[\frac{\partial v_z}{\partial r}+\frac{\partial v_r}{\partial z}\right].$$

The divergence of velocity vector v in 2D-cylindrical coordinates is given by

$$\nabla\cdot\boldsymbol{v}=\frac{\partial v_z}{\partial z}+\frac{1}{r}\frac{\partial}{\partial r}(rv_r). \quad (3)$$

The system of Eqs. (1) and (2) is subject to the following boundary conditions:

$$\begin{aligned} &v_z(r=R_0,z,t)=0, \quad v_z(r,z=0,t)=v_0,\\ &v_r(r=0,z,t)=0, \quad v_r(r=R_0,z,t)=0,\\ &p(r,z=L,t)=p_0,\\ &\left.\frac{\partial v_z}{\partial r}\right|_{r=0,z,t}=0. \end{aligned} \quad (4)$$

In the above equations, v_0 is the fluid axial-velocity at the inlet and p_0 is the pressure at the outlet. As mentioned before, the formation of the solid wax produces interlocked platelets with liquid in the solid pore space resulting in gel formation. Due to crystallization, a moving solid–liquid boundary forms. The major challenge is how to account for the deceleration of the fluid flow in the gel region with a fixed grid. Voller et al. [17,18,21] have introduced an enthalpy–porosity approach to simulate freezing of liquids in a thermal cavity. The enthalpy–porosity approach treats the phase change as a pseudo-porous medium with porosity, ε, decreasing from 1 to 0 as the solid fraction increases from 0 to 1. A Darcy-type source term is added to the momentum equations in order to describe the velocity deceleration in the mushy region.

In this work, we adopt the enthalpy–porosity approach to model the bulk flow in the gel layer and add the following source terms:

$$S_z=-Av_z, \quad (5)$$
$$S_r=-Av_r \quad (6)$$

to the right-hand side of Eqs. (1) and (2), respectively. In the liquid region, the source terms are set to zero. In the gel layer (where liquid is trapped in the wax platelets), the parameter A is large enough such that the source terms dominate the transient, convective, and diffusive terms and thus the momentum equation approximates Darcy's law. As the solid saturation increases to one, the source terms dominate all the other terms in the momentum equation, and forces the liquid velocities close to zero. The source term is thus a function of the porosity of the gel medium (i.e., the wax saturation). One way to define a suitable form for A is to use the Carman–Koseny equation [21]. The Car-

man–Koseny equation relates the effective permeability K to the porosity ε through the equation [30]:

$$K = \frac{1}{C}\frac{\varepsilon^3}{(1-\varepsilon)^2}, \tag{7}$$

where C is the morphology coefficient. Darcy's law can then be approximated by

$$\nabla p = -\frac{\mu}{K}\boldsymbol{v} \approx -C\mu\frac{(1-\varepsilon)^2}{\varepsilon^3}\boldsymbol{v}. \tag{8}$$

From Eq. (8) we obtain

$$A = -C\mu\frac{(1-\varepsilon)^2}{\varepsilon^3+q}. \tag{9}$$

The value of C depends on the morphology of the porous media. As an example for a packed bed of spheres $C = 150/Dp^2$, where Dp is the sphere diameter; with this expression and Eq. (7) one can estimates an accurate value for permeability [31]. For metal formation with grains of $Dp = 1$ mm a value of $C = 10^3\ \mathrm{m}^{-2}$ is obtained; this value was used for the Gallium solidification study [21]. For wax morphology we find $C = 10^6\ \mathrm{m}^{-2}$ for describing flow in the gel layer as we will comment in Hoteit et al. [32].

3.2. Energy balance

The general form of the energy equation for a single phase, multicomponent mixture can be written as [28]:

$$\frac{\partial}{\partial t}\left(\sum_{i=1}^{n} c_i\overline{H}_i\right) = -\nabla\cdot\boldsymbol{e} + \frac{DP}{Dt} + \mathbf{T}:\nabla\boldsymbol{v}, \tag{10}$$

where $\overline{H}_i$ is the partial molar enthalpy of component i, and DP/Dt is the energetic contribution of the pressure due to expansion or compression. The term $\mathbf{T}$ is the stress tensor and $\mathbf{T}:\nabla\boldsymbol{v}$ is the energetic contribution of viscous dissipation. The term $\boldsymbol{e}$ is the *multicomponent energy flux* relative to fixed coordinates; it is defined as [28]:

$$\boldsymbol{e} \equiv \boldsymbol{v}\sum_{i=1}^{n} c_i\overline{H}_i + \boldsymbol{q}. \tag{11}$$

The term $\boldsymbol{v}\sum_{i=1}^{n} c_i\overline{H}_i$ is the energy flux due to convection. The term $\boldsymbol{q}$ is given by [28]:

$$\boldsymbol{q} = -k\nabla T + \sum_{i=1}^{n}\boldsymbol{J}_i\overline{H}_i + \boldsymbol{q}^{(x)}, \tag{12}$$

where $-k\nabla T$ is the energy flux due to conduction and the term $\sum_{i=1}^{n}\boldsymbol{J}_i\overline{H}_i$ represents energy transfer due to diffusion of species. The term $\boldsymbol{q}^{(x)}$ represents the Dufour or *diffusion-thermo* effect, which is usually negligible. Neglecting the energetic contributions of the pressure DP/Dt, viscous dissipation $\mathbf{T}:\nabla\boldsymbol{v}$, and the inter-diffusion of enthalpy $\sum_{i=1}^{n}\boldsymbol{J}_i\overline{H}_i$, the energy equation for the single-phase liquid flow can be written as

$$\frac{\partial}{\partial t}\left(\sum_{i=1}^{n} c_i\overline{H}_i\right) + \nabla\cdot\sum_{i=1}^{n} c_i\overline{H}_i\boldsymbol{v} = \nabla\cdot(k\nabla T). \tag{13}$$

The energy equation in the gel layer is written in terms of the enthalpies of liquid and solid phases:

$$\frac{\partial}{\partial t}\left(\sum_{j=\mathrm{o,s}} S_j c_j H_j\right) + \nabla.\left(\sum_{j=\mathrm{o,s}} S_j c_j H_j\boldsymbol{v}_j\right) = \nabla\cdot(k_{\mathrm{eff}}\nabla T), \tag{14}$$

where the index $j = \mathrm{o, s}$ refers to the oil phase and wax phase (solid phase), respectively; H_j and S_j are, respectively, the molar enthalpy and volume fraction (saturation) of phase j, and k and k_{eff} are the liquid thermal conductivity in the single phase liquid region and the effective thermal conductivity in the gel layer, respectively.

The energy equation is subject to the following boundary conditions:

$$T(R_0,z,t) = T_{\mathrm{a}}, \quad T(r,0,t) = T_{\mathrm{in}}, \quad \left.\frac{\partial T}{\partial r}\right|_{r=0,z,t} = 0, \quad \left.\frac{\partial T}{\partial z}\right|_{r,z=L,t} = 0. \tag{15}$$

The last expression in Eq. (15), which ignores the axial thermal conduction at the outlet, is based on a pseudo-steady state assumption. The effective thermal conductivity k_{eff} in Eq. (14) can be calculated from the Maxwell correlation [33]:

$$k_{\mathrm{eff}} = \frac{[2k_{\mathrm{o}} + k_{\mathrm{s}} - 2S_{\mathrm{s}}(k_{\mathrm{o}} - k_{\mathrm{s}})]}{[2k_{\mathrm{o}} + k_{\mathrm{s}} + S_{\mathrm{s}}(k_{\mathrm{o}} - k_{\mathrm{s}})]}k_{\mathrm{o}}. \tag{16}$$

One may use other models in the calculation of the effective thermal conductivity of a two-phase mixture [34]. The molar enthalpy of the oil phase can be calculated from the PR-EOS [35]:

$$H_{\mathrm{o}}(T,p,\boldsymbol{x}_{\mathrm{o}}) = H^*(T,0,\boldsymbol{x}_{\mathrm{o}}) + RT(Z-1) + \left(\frac{T}{2\sqrt{2}b}\frac{\mathrm{d}a(T)}{\mathrm{d}T} - \frac{a(T)}{2\sqrt{2}b}\right)\ln\frac{Z+2.414B}{Z-2.414B}, \tag{17}$$

where $Z = pv_{\mathrm{o}}/RT$ is the compressibility factor of the oil phase and $H^*(T,0,\boldsymbol{x}_{\mathrm{o}})$ is the ideal gas enthalpy of liquid mixture at zero pressure, which can be calculated from:

$$H^*(T,0,\boldsymbol{x}_{\mathrm{o}}) = \sum_{i=1}^{n} x_{\mathrm{o},i}H_i^*(T,0). \tag{18}$$

In Eq. (18), $H_i^*(T,0)$ is the ideal gas enthalpy of component i. Passut and Danner [36] provide correlations for ideal gas enthalpy of some 90 substances.

We use the following expression to calculate the enthalpy of the solid wax:

$$H_{\mathrm{s}}(T,p,\boldsymbol{x}_{\mathrm{s}}) = \sum_{i=1}^{n} x_{\mathrm{s},i}H_{\mathrm{s},i}(T,p). \tag{19}$$

Assuming that pressure has negligible effect on the molar enthalpy of the solid, and neglecting the effect of tempera-

ture variation on heat capacity of component i in the solid state, we can write [35]:

$$H_{s,i}(T,p) \approx H_{s,i}(T,p_i^{\mathrm{f}}) \approx H_{s,i}(T_i^{\mathrm{f}},p_i^{\mathrm{f}}) + Cp_{s,i}(T - T_i^{\mathrm{f}}). \quad (20)$$

From the definition of molar latent heat of component i (heat of fusion):

$$\lambda_i = H_{\mathrm{o},i}(T_i^{\mathrm{f}},p_i^{\mathrm{f}}) - H_{\mathrm{s},i}(T_i^{\mathrm{f}},p_i^{\mathrm{f}}). \quad (21)$$

Eqs. (19)–(21) are combined to obtain

$$H_{\mathrm{s}}(T,P,\boldsymbol{x}_{\mathrm{s}}) = \sum_{i=1}^{n} x_{\mathrm{s},i}[H_{\mathrm{o},i}(T_i^{\mathrm{f}},p_i^{\mathrm{f}}) - \lambda_i + Cp_{\mathrm{s},i}(T - T_i^{\mathrm{f}})]. \quad (22)$$

In this work, the terms $\lambda_i, H_{\mathrm{o},i}(T_i^{\mathrm{f}},p_i^{\mathrm{f}})$, and $Cp_{\mathrm{s},i}$ are assumed constant; λ_i can be evaluated as the average value at T and T_i^{f}.

3.3. Species balance

The gel layer has structure of platelets that overlap and interlock and may contain up to 98% liquid in early time of deposition [23,24,37]. The gel layer may grow with time. Let us consider flow in two-phase in the domain and write the mass balance of species i:

$$\frac{\partial}{\partial t}\sum_{j=\mathrm{o,s}}(S_j c_{j,i}) + \nabla.\sum_{j=\mathrm{o,s}}(S_j c_{j,i}\boldsymbol{v}_{j,i}) = 0, \quad i = 1,\ldots,n, \quad (23)$$

where $c_{j,i}$ and $\boldsymbol{v}_{j,i}$ are the molar density of component i in phase j, and the velocity vector for component i in phase j, respectively. The relation between the bulk velocity, $\boldsymbol{v}_j$ of phase j, molar diffusive flux, $\boldsymbol{J}_{j,i}$, and velocity of component i in phase j, $\boldsymbol{v}_{j,i}$ is given by

$$S_j c_{j,i}\boldsymbol{v}_{j,i} = S_j c_{j,i}\boldsymbol{v}_j + S_j\boldsymbol{J}_{j,i}, \quad i = 1,\ldots,n. \quad (24)$$

Substitution of Eq. (24) into Eq. (23) yields

$$\frac{\partial}{\partial t}\sum_{j=\mathrm{o,s}}(S_j c_j x_{j,i}) + \nabla\cdot\sum_{j=\mathrm{o,w}}(S_j c_j x_{j,i}\boldsymbol{v}_j + S_j\boldsymbol{J}_{j,i}) = 0, \quad i = 1,\ldots,n, \quad (25)$$

where c_j and $x_{j,i}$ are the molar density of phase j and mole fraction of component i in phase j. The molar density of phase j and molar density of component i in phase j are related by

$$c_{j,i} = x_{j,i}c_j. \quad (26)$$

Note that in each phase

$$\sum_{i=1}^{n}(\boldsymbol{J}_{j,i}) = 0, \qquad j = \mathrm{o,s}. \quad (27)$$

By summing Eq. (25) for $i = 1,\ldots,n$ and using $\sum_{i=1}^{n} x_{j,i} = 1$; $j = \mathrm{o,s}$, and Eq. (27), the total molar balance expression is given by

$$\frac{\partial}{\partial t}\sum_{j=\mathrm{o,s}}(S_j c_j) + \nabla\cdot\sum_{j=\mathrm{o,s}}(S_j c_j\boldsymbol{v}_j) = 0. \quad (28)$$

The total molar density c is defined by

$$c = \sum_{j=\mathrm{o,s}} S_j c_j. \quad (29)$$

The overall composition of component i is related to the phase composition of component i by

$$cz_i = \sum_{j=\mathrm{o,s}} S_j c_j x_{j,i}, \quad i = 1,\ldots,n. \quad (30)$$

Using Eq. (30) one can write Eq. (28) as

$$\frac{\partial}{\partial t}(cz_i) + \nabla\cdot\sum_{j=\mathrm{o,s}}(S_j c_j x_{j,i}\boldsymbol{v}_j + S_j\boldsymbol{J}_{j,i}) = 0, \quad i = 1,\ldots,n. \quad (31)$$

The total molar balance from Eq. (31) can be written as

$$\frac{\partial c}{\partial t} + \nabla\cdot\sum_{j=\mathrm{o,s}}(S_j c_j x_{j,i}\boldsymbol{v}_j) = 0, \quad i = 1,\ldots,n. \quad (32)$$

Eqs. (31) and (32) are subject to the following boundary conditions:

$$\begin{aligned} &z_i = (z_i)_{\mathrm{in}} \quad \text{at } z = 0,\\ &(\boldsymbol{J}_{j,i})_r = 0 \quad \text{at } r = 0, R_0,\\ &\frac{\partial z_i}{\partial r} = 0 \quad \text{at } r = 0. \end{aligned} \quad (33)$$

3.3.1. Diffusion flux

The molar diffusion flux in a vector form can be written as [38]:

$$\boldsymbol{J} = -c(\boldsymbol{D}^{\mathrm{M}}\nabla x + \boldsymbol{D}^{\mathrm{T}}\nabla T + \boldsymbol{D}^{\mathrm{P}}\nabla p). \quad (34)$$

where $\boldsymbol{J}$, $\boldsymbol{D}^{\mathrm{M}}$, $\boldsymbol{D}^{\mathrm{T}}$ and $\boldsymbol{D}^{\mathrm{P}}$ are the total diffusion flux vector, molecular diffusion coefficient matrix, thermal diffusion coefficient vector, and pressure diffusion coefficient vector, respectively. On the right side, the first, second, and third terms represent molecular diffusion, thermal diffusion, and pressure diffusion, respectively. Neglecting the pressure diffusion, the diffusion flux of component i, $i = 1,\ldots,n-1$, in phase j is given by

$$\boldsymbol{J}_j = -c_j(\boldsymbol{D}_j^{\mathrm{M}}\nabla\boldsymbol{x}_j + \boldsymbol{D}_j^{\mathrm{T}}\nabla T). \quad (35)$$

where $\boldsymbol{J}_j = [\boldsymbol{J}_{j,i}]$ and $\nabla\boldsymbol{x}_j = [\nabla\boldsymbol{x}_{j,i}]$; $\boldsymbol{D}_j^{\mathrm{M}} = [D_{j,i,k}^{\mathrm{M}}], k = 1,\ldots,n-1$ and $\boldsymbol{D}_j^{\mathrm{T}} = [D_{j,i}^{\mathrm{T}}]$ are the molecular diffusion coefficients and the thermal diffusion coefficients in phase j, respectively. Firoozabadi et al. [38,39] describe the methodology for calculating molecular and thermal diffusion coefficients. Eq. (35) consists of two terms. The first term on the right side is known as the Fick's law and the second term is often referred to as the Soret effect. In a multicomponent mixture such as a petroleum fluid with varying molecular sizes and molecular shapes, in addition to diagonal molecular diffusion coefficients, cross coefficients may become important [40].

To the best of our knowledge, in all of the existing models for wax deposition, the diffusion flux in a (pseudo)

binary mixture in the radial direction is written in the following form:

$$J_{o,1} = -cD^{M}_{o,1,1}\frac{\partial z_1}{\partial r} = -cD^{M}_{o,1,1}\frac{\partial z_1}{\partial T}\frac{\partial T}{\partial r}. \quad (36)$$

The concentration gradient in the Fick's law of diffusion is subject to constant temperature and pressure and thus the expression above is not valid. The appropriate form of the diffusion flux without pressure diffusion is given by Eq. (35).

3.4. Solid–liquid equilibria

There are two types of models for wax precipitation calculations in petroleum fluids; (1) solid solution, and (2) multisolid-phase. The multisolid model can describe the WAT and the amount of precipitation more accurately than the solid solution model [41,42]. In this work, we perform the solid–liquid phase calculations by using the multisolid-phase model by Lira-Galeana et al. [6], where each precipitated component forms a solid layer, which does not mix with the other solid layers. The model uses a two-step procedure for the phase-split calculation:

(1) Stability analysis.
(2) Phase-split calculation.

3.4.1. Stability analysis

This is a preprocessing step to identify which of the components are precipitating and which are not. A component i precipitates at a given temperature and pressure if the following condition is satisfied [33]:

$$f_i(p,T,z) - f^{pure}_{s,i}(p,T) \geqslant 0, \quad (37)$$

where $f_i(p,T,z)$ and $f^{pure}_{s,i}(p,T)$ are the fugacity of component i with overall composition z, and fugacity of pure solid-component i at pressure p and temperature T, respectively.

3.4.2. Phase-split calculation

Suppose the stability-analysis provides the condition that n_s components of the n-component mixture (i.e., the components $(n-n_s+1),\ldots,n$) precipitate. These components, therefore, fulfill Eq. (37).

The governing equations for the wax precipitation are given by the equilibrium and the material balance equations. For every precipitating component i, the equilibrium and material balance equations are, respectively, given by

$$f_{o,i}(p,T,\boldsymbol{x}_o) = f^{pure}_{s,i}(p,T), \quad i = (n-n_s+1),\ldots,n, \quad (38)$$

and

$$z_i - x_{o,i}\left[1 - \sum_{k=n-n_s+1}^{n}\frac{N_{s,k}}{F}\right] - \frac{N_{s,i}}{F} = 0, \quad i = (n-n_s+1),\ldots,n. \quad (39)$$

The material balance equations for the non-precipitating components are

$$z_i - x_{o,i}\left[1 - \sum_{k=n-n_s+1}^{n}\frac{N_{s,k}}{F}\right] = 0, \quad i = 1,\ldots,(n-n_s), \quad (40)$$

where $f_{o,i}(p,T,\boldsymbol{x}_o)$ is the fugacity of component i in the oil phase with composition $x_{o,i}$, $N_{s,i}$ is the number of moles of component i in the wax phase, F is the total number of moles of the wax components.

The fugacities of a pure component i in solid and liquid states are related by [33]:

$$f^{pure}_{s,i}(p,T) = f^{pure}_{o,i}(p,T)\exp[-\Delta\mu_i], \quad (41)$$

where $\Delta\mu_i = \mu^{pure}_{o,i} - \mu^{pure}_{s,i}/RT = \left(\Delta h^f_i/RT^f_i - \Delta Cp_i/RT^f_i\right)\left(T^f_i/T - 1\right) - \Delta Cp_i/RT^f_i \ln\left(T^f_i/T\right)$.

The symbols are defined in the Nomenclature. The fugacity of pure component i in the liquid state can be calculated from the Peng–Robinson equation of state.

4. Numerical model

The momentum, energy, and species mass balance equations and the local wax solid–liquid model are coupled and solved with initial and boundary conditions to predict the pressure, temperature, velocity and composition in the gel and liquid regions as well as the wax fraction (i.e., volume fraction or weight fraction). The 2D computational domain is discretized into a structured grid of rectangular elements. A finite-volume based method is used for the spatial approximations. Different temporal, spatial and linearization schemes are implemented to solve the governing equations. The scalar unknowns like the pressure, temperature, enthalpies, densities, mole fractions and saturation are approximated over the same control volumes while the velocity is approximated over a different control volume. The numerical algorithm uses two levels of iterations at each time step. In the inner level, we solve the coupled momentum and total mass balance equations to approximate the pressure and the velocity field. In the outer level, we solve the energy equation and the species balance equations to calculate the temperature and the overall composition. Once the overall composition, temperature, and pressure are known, we apply the phase-equilibria model to calculate the oil and wax compositions and the wax saturation in the gel layer.

Here, we provide the basic numerical methods used to solve our system of equations.

4.1. Solution of the momentum equation

The momentum equation is solved by using the SIMPLER method of Patankar [43]. In this method, a "staggered" or a displaced grid for the velocity components is used. The velocity components are calculated for the points that lie on the faces of the control volumes and the pressure at the main grid points (see Fig. 3). For presentational convenience, the general discretization of axial and radial momentum equations (combined Eqs. (1) and (5), and

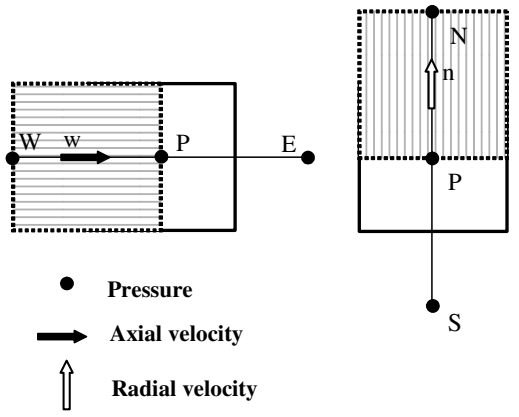

Fig. 3. Computational cells, discretization and staggered model based on SIMPLER method.

Eqs. (2) and (6)) at the west- and north-cell faces of a scalar control volume P are given by:

$$(A_z^{\mathrm{w}} + \overline{S}_z^{\mathrm{w}})v_z^{\mathrm{w}} = \sum_{nb} a_z^{\mathrm{nb}} v_z^{\mathrm{nb}} + (p^{\mathrm{P}} - p^{\mathrm{w}})a_z^{\mathrm{w}} + b_z{}^{\mathrm{w}}, \tag{42}$$

and

$$(A_r^{\mathrm{n}} + \overline{S}_r^{\mathrm{n}})v_r^{\mathrm{n}} = \sum_{\mathrm{nb}} a_r^{\mathrm{nb}} v_r^{\mathrm{nb}} + (p^{\mathrm{P}} - p^{\mathrm{N}})a_r^{\mathrm{n}} + b_r{}^{\mathrm{n}}. \tag{43}$$

The spatial, temporal and fluid dependant terms are incorporated into the coefficients A, a and b in Eqs. (42) and (43). These coefficients are calculated by using the *power law* scheme of Patankar [41]. The subscript *nb* refers to the neighboring nodes of the control volume P. The discretized Eqs. (42) and (43) are similar to the general discretized equations defined by Patankar except in two additional terms $\overline{S}_z^{\mathrm{w}}$ and $\overline{S}_r^{\mathrm{n}}$ [43]. These terms, which appear on the right-hand side of Eqs. (42) and (43), are a consequence of the added Darcy-type source term to the momentum equations. Note that these terms end up at the diagonal of the linear system whose solution is the velocity field. The values of the axial and radial velocities are thus inversely proportional to $\overline{S}_z^{\mathrm{w}}$ and $\overline{S}_r^{\mathrm{n}}$, respectively.

The discretization of the momentum equations leads to two equations and three unknowns; p, v_z, and v_r. To close the system, Eqs. (42) and (43) are coupled with the total molar conservation equation. Assuming that the solid phase does not flow, the total molar conservation equation becomes

$$\frac{\partial c}{\partial t} + \nabla \cdot (S_{\mathrm{o}} c_{\mathrm{o}} \boldsymbol{v}_{\mathrm{o}}) = 0. \tag{44}$$

A finite-volume method is used to discretize Eq. (44). The scalar variables S_{o}, c_{o} and c are approximated over the same control volumes as the pressure. The spatial and temporal discretization of Eq. (44) can be written in the general form as

$$\sum_{\mathrm{nb}} \bar{a}_z^{\mathrm{nb}} v_z^{\mathrm{nb}} + \sum_{\mathrm{nb}} \bar{b}_r^{\mathrm{nb}} \boldsymbol{v}_r^{\mathrm{nb}} = \frac{(c^n - c^{n-1})}{\Delta t}. \tag{45}$$

A first-order upwind scheme is used to define the coefficients $\bar{a}_z^{\mathrm{nb}}$ and $\bar{b}_r^{\mathrm{nb}}$ at the control volume boundaries. These coefficients with the right-hand term in Eq. (45) are evaluated from the information at previous time steps. The sought unknowns from Eqs. (42)–(44) are the velocities v_z and v_r, and the pressure. A full description of the algorithm can be found in Refs. [43,44].

4.2. Solution of the energy equation

Assuming that the solid wax phase is immobile, the energy balance equation, Eq. (14) simplifies to

$$\frac{\partial}{\partial t}\left(\sum_{j=\mathrm{o,s}} S_j c_j H_j\right) + \nabla.(S_{\mathrm{o}} c_{\mathrm{o}} H_{\mathrm{o}} \boldsymbol{v}_{\mathrm{o}}) = \nabla \cdot (k_{\mathrm{eff}} \nabla T). \tag{46}$$

The finite-volume method is used for the spatial discretization of Eq. (46). The convection term, which is the second term in the left-hand side of Eq. (46) is solved by using a first-order upwind scheme. The left-hand side of Eq. (46) representing heat conduction is approximated by a central finite difference scheme. The time operator is approximated by a semi-implicit time scheme. The enthalpies H_{o} and H_{s}, and the temperature T are implicit in time. The other variables are known from the previous time step iteration. The spatial and temporal discretization of Eq. (46) over a control volume P can be written in the form (see the Appendix):

$$G_{\mathrm{P}}(T) \equiv a_{\mathrm{o,}P} H_{\mathrm{o,P}} + a_{\mathrm{s,P}} H_{\mathrm{s,P}} - \sum_{\mathrm{nb}} F_{\mathrm{nb}} H_{\mathrm{nb}} - \sum_{\mathrm{nb}} D_{\mathrm{nb}} T_{\mathrm{nb}} - b_{\mathrm{P}} = 0. \tag{47}$$

The coefficients $a_{\mathrm{o,P}}$,$a_{\mathrm{w,P}}$,b_{P},F_{nb} and D_{nb} are calculated from information at the previous iterations (see the Appendix). The enthalpies in Eq. (47) are functions of temperature and composition; they are defined in Eqs. (17) and (19). The linearization of Eq. (47) by the Newton–Raphson (NR) method yields

$$(a_{\mathrm{o,P}} Cp_{\mathrm{o,P}} + a_{\mathrm{s,P}} Cp_{\mathrm{s,P}})\Delta T_{\mathrm{P}} - \sum_{\mathrm{nb}} (F_{\mathrm{nb}} Cp_{\mathrm{nb,P}} + D_{\mathrm{nb}})\Delta T_{\mathrm{nb,P}} = -G_{\mathrm{P}}(T^{\ell-1}), \tag{48}$$

where ℓ refers to the iteration counter and $Cp_{\mathrm{o,nb}} = \partial H_{\mathrm{o,nb}}/\partial T$, $Cp_{\mathrm{s,nb}} = \partial H_{\mathrm{s,nb}}/\partial T$. The main steps of the algorithm are:

1. For given velocities, densities, and saturation compute the coefficients $a_{\mathrm{o,P}}$,$a_{\mathrm{s,P}}$,F_{nb} and D_{nb}.
2. For given pressure, temperature and composition apply the PR-EOS and calculate the derivatives $\partial H_{\mathrm{o}}/\partial T$ and $\partial H_{\mathrm{s}}/\partial T$.
3. Solve the linear system given in Eq. (47) and correct the temperature from $T^{\ell} = T^{\ell-1} + \Delta T$.
4. Repeat steps 1–3 until the convergence criterion $\|\Delta T\| < \mathrm{TOL}$ is satisfied.

4.3. Solution of the species balance equations

Neglecting the velocity and diffusion in the solid phase and using Eq. (31), the species balance can be written as

$$\frac{\partial}{\partial t}(cz_i) + \nabla\cdot(cv_o z_i) = -\nabla\cdot(S_o \boldsymbol{J}_{o,i}) + \nabla\cdot(S_s c_s x_{s,i}\boldsymbol{v}_o), \quad i = 1,\ldots,n. \tag{49}$$

The finite-volume scheme is also used for the spatial discretization of the species balance equations. The convection term in the left-hand side of Eq. (49) is treated implicitly in time with a first-order upwinding scheme. The terms on the right-hand side are calculated explicitly.

4.4. Solution of the phase-equilibria model

The stability analysis can be readily performed by using the PR-EOS and the expression of the fugacity of the wax phase given in Eq. (41). The phase-split calculation can be performed efficiently by using the *successive-substitution-iteration* (SSI) or the NR methods. Here, we provide the algorithms for the phase-split calculation by both methods.

The governing system has $(n + n_s)$ equations given by Eqs. (38)–(40) and $(n + n_s)$ unknowns, which are the mole fraction of the oil phase $(x_{o,i};\ i = 1,\ldots,n)$ and the number of mole of the precipitated wax components $(N_{s,i};\ j = (n - n_s + 1),\ldots,n)$.

The main steps of the SSI algorithm are as follows:

1. Guess an initial oil mole fraction $\boldsymbol{x}_o^{old}$. If no information is available, take the oil mole fraction to be the same as the feed mole fraction (i.e., $\boldsymbol{x}_o^{old} = z$).
2. Calculate the fugacity $f_{o,i}(p, T, \boldsymbol{x}_o^{old})$ from the PR-EOS.
3. Update the oil mole fraction of the precipitating components from (see Eq. (38)):

$$x_{o,i} = \frac{f_{s,i}(p,T)}{f_{o,i}(p,T,\boldsymbol{x}_o^{old})} x_{o,i}^{old}, \quad i = (n - n_s + 1),\ldots,n.$$

4. Define N_s from

$$N_s = \sum_{j=n-n_s+1}^{n} \frac{N_{s,j}}{F}.$$

N_s can be calculated by summing Eq. (39) for $i = (n - n_s + 1),\ldots,n$, that is,

$$N_s = \frac{Z_s - X_o}{1 - X_o},$$

where $X_o = \sum_{i=n-n_s+1}^{n} x_{o,i}$ and $Z_s = \sum_{i=n-n_s+1}^{n} z_i$.

5. Use Eq. (39) to calculate the number of moles of the precipitating components

$$N_{s,i} = z_i - x_{o,i}[1 - N_s], \quad i = (n - n_s + 1),\ldots,n.$$

6. Use Eq. (40) to calculate the oil mole fractions of the non-precipitating components

$$x_{o,i} = \frac{z_i}{1 - N_s}, \quad i = 1,\ldots,(n - n_s).$$

7. Normalize the oil mole fraction $x_{o,i}$.
8. Check if the convergence criterion $\|\boldsymbol{x}_o - \boldsymbol{x}_o^{old}\| < \text{TOL}$ is satisfied. If not, set $\boldsymbol{x}_o^{old} = \boldsymbol{x}_o$ and repeat steps 2–8.

The computational speed of each SSI iteration is quite fast but generally it requires more iterations than the NR method. In the NR algorithm, we define the residual function g_i from (see Eq. (38)),

$$g_i(\boldsymbol{x}_o) \equiv f_{o,i}(p,T,\boldsymbol{x}_o) - f_{s,i}(p,T) = 0, \quad i = (n - n_s + 1),\ldots,n. \tag{50}$$

The composition of the precipitating components is then computed by solving:

$$\overline{\boldsymbol{J}}\Delta\boldsymbol{x}_o = -\boldsymbol{G}, \tag{51}$$

where

$$\overline{\boldsymbol{J}} = \left[\frac{\partial g_i}{\partial \boldsymbol{x}_{o,j}}\right]_{i,j=(n-n_s+1),\ldots,n}, \quad \Delta x_o = [\boldsymbol{x}_i]_{i=(n-n_s+1),\ldots,n}, \quad \text{and} \quad \boldsymbol{G} = -[g_i]_{i=(n-n_s+1),\ldots,n}.$$

Note that the size of the linear system is equal to the number of precipitating components. The mole fractions of the oil phase for the precipitating components are then updated from

$$x_{o,i} = x_{o,i}^{old} + \Delta x_{o,i}, \quad i = (n - n_s + 1),\ldots,n. \tag{52}$$

The NR algorithm is similar to SSI algorithm described above and is implemented by replacing the update of the composition of the precipitating components in Eq. (52) by step 3 in the SSI algorithm. The other steps are exactly the same.

In all our calculations, even very close to phase boundaries, the SSI method performed very well. Unlike vapor-liquid equilibria calculations, where close to phase boundaries the SSI algorithm becomes inefficient, there was no convergence problem with the SSI algorithm in the entire saturation range in wax precipitation calculations.

5. General algorithm

The main steps of the algorithm for predicting the wax deposition in pipelines are the following:

- Initialize the fluid and pipe parameters.
- Iterate over the time step (outer loop).
  1. Update the diffusion coefficients and the fluid viscosity.
  2. Iterate until convergence (inner loop).
     - 2.1 Solve the momentum and the total mass balance equations to approximate the pressure and velocity field.
     - 2.2 Solve the energy equation to calculate the temperature.

2.3 Solve the species balance equations to calculate the overall composition.
2.4 Set $c^{\text{old}} = c$, where c is the overall density.
2.5 Apply the phase-equilibria model to calculate phase compositions, saturation, and oil, wax and overall densities.
2.6 Check the convergence criterion $\|c^{\text{old}} - c\| < \text{TOL}$. If no convergence, repeat steps 2.1–2.6.

– Repeat until the assigned time is reached.

The fluid viscosity is a function of temperature, pressure and composition. It is calculated from the correlation of Lohrentz et al. [45]. The diffusion coefficients and the viscosity are updated outside the inner loop for their weak dependency on the temperature and pressure variation during the convergence process of the inner loop.

6. Summary and concluding remarks

A mathematical model for wax deposition in pipelines for a multicomponent fluid is presented. The model couples the momentum, energy and species balance equations and a multisolid-wax precipitation model. There are two main features that characterize our model:

1. We include molecular diffusion and thermal diffusion in our formulation. Both affect the flux of species towards the pipe wall by diffusion. The driving force for molecular diffusion is the concentration gradient. The driving force for thermal diffusion is temperature gradient. These two gradients may not be proportional in the gel layer. The temperature gradient is expected to be high close to the pipe wall. The concentration gradient, because of phase change, is expected to be high close to the interface of the single liquid phase region and the gel layer. Furthermore the temperature gradient close to the wall may reach a pseudo steady state quickly and stay large close to the wall. This may not be true for the concentration gradients. All these aspects may lead to incorrect results by the commonly accepted use of the chain rule to replace concentration gradient by temperature gradient in the Fick's law. In Hoteit et al. [32], the numerical results will demonstrate the importance of the use of the proper diffusion flux expression and the need for consistency in diffusion flux expression from irreversible thermodynamics. With consistent formulation the model is predictive.
2. An enthalpy–porosity approach is used to account for the flow deceleration in the gel layer where it is modeled as a pseudo-porous medium. A Darcy-type source term is added to the momentum equations. This source term is a function of the porosity (oil saturation) in the gel layer. In the single-phase liquid region, this function is set to zero and the velocity is calculated from the momentum equation. In the gel layer, the source term increases gradually with a Carman–Koseny-type function as the solid saturation increases. The velocity field is inversely proportional to source function. The increase in the source term leads to a decrease in the velocity field. The energy equation is written in terms of the liquid and solid enthalpies.

A detailed numerical algorithm to solve the mathematical model is also provided. The momentum equation coupled with the total mass balance equation is solved by the SIMPLER method to approximate the pressure and velocity field. The energy equation is discretized by a finite volume scheme and linearized by the NR method. The liquid enthalpy is related to temperature using the PR-EOS. A robust algorithm for solid–liquid equilibria is presented. The algorithm uses the SSI method or the NR method. With the NR method, the size of the linear system is the number of precipitating components which makes the algorithm very efficient.

Acknowledgements

The funding for this work was provided by the member companies of the Reservoir Engineering Research Institute (RERI). We thank Daniel Rosner and Alana Leahy-Dios of Yale University for reading the paper and their comments.

Appendix A

The energy balance equation (Eq. (46)), in cylindrical coordinates, is written as

$$\frac{\partial}{\partial t}\left(\sum_{j=\text{o,s}} S_j c_j H_j\right) + \frac{\partial}{\partial z}(J_z) + \frac{1}{r}\frac{\partial}{\partial r}(J_r) = 0, \tag{A.1}$$

where

$$J_z = \left(S_\text{o} c_\text{o} H_\text{o} v_{\text{o},z} - k_\text{eff}\frac{\partial T}{\partial z}\right) \quad \text{and}$$

$$J_r = r\left(S_\text{o} c_\text{o} H_\text{o} v_{\text{o},r} - k_\text{eff}\frac{\partial T}{\partial r}\right).$$

Let P be a control volume with edges e, w, n and s, and neighboring control volumes E, W, N, and S. Fig. A1 illustrates the five point grid cluster at P. For the sake of simplicity, we suppose that the domain is uniformly discretized with space steps Δz and Δr along the z- and r-directions, respectively (Fig. A1).

Integrating Eq. (A.1) over the control volume P, we get the semi-discretized equation:

$$\frac{\partial}{\partial t}\left(\sum_{j=\text{o,s}} S_j c_j H_j\right)_\text{P} \Delta z \Delta r + J_\text{e} - J_\text{w} + J_\text{n} - J_\text{s} = 0. \tag{A.2}$$

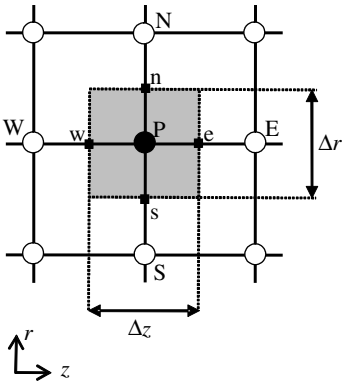

Fig. A1. Grid point cluster at location P. Staggered discretization method to implement SIMPLER algorithm. Scalar variables are presented at the center of the control volume. Vector variables are located at the surface of control volume.

The fluxes J_e, J_w, J_n, and J_s in Eq. (A.2) are defined by

$$J_e = \widetilde{F}_e H_{o,e} - D_e(T_E - T_P), \quad J_w = \widetilde{F}_w H_{o,w} - D_w(T_P - T_W),$$
$$J_n = \widetilde{F}_n H_{o,n} - D_n(T_N - T_P), \quad J_s = \widetilde{F}_s H_{o,s} - D_s(T_P - T_S),$$

where

$$\begin{cases} \widetilde{F}_{nb} = (S_o c_o v_{o,z})_{nb} \Delta r \\ D_{nb} = (k_{eff})_{nb} \frac{\Delta r}{\Delta z} \end{cases} \text{for nb} = \text{w, e, and}$$
$$\begin{cases} \widetilde{F}_{nb} = \frac{r_{nb}}{r_P} (S_o c_o v_{o,z})_{nb} \Delta z \\ D_{nb} = \frac{r_{nb}}{r_P} (k_{eff})_{nb} \frac{\Delta z}{\Delta r} \end{cases} \text{for nb} = \text{n, s.}$$

Different schemes, such as *upstream*, *hybrid*, and *power law* can be used to define the variables at the interfaces between the blocks [43]. By using the upstream scheme, the semi-discretized Eq. (A.2) is written in the general form:

$$\frac{\partial}{\partial t}\left(\sum_{j=o,s} S_j c_j H_j\right)_P \Delta z \Delta r = \sum_{nb} F_{nb} H_{o,nb} + \sum_{nb} D_{nb} T_{nb}, \tag{A.3}$$

The counter nb in the above equation refers to the center and edge points P, e, w, n and s. The coefficient F_{nb} and D_{nb} are defined as

$$F_e = \max(-\widetilde{F}_e, 0), \quad F_w = \max(\widetilde{F}_w, 0), F_n = \max(-\widetilde{F}_n, 0),$$
$$F_s = \max(-\widetilde{F}_s, 0), \quad F_P = -\sum_{nb=n,w,e,s} F_{nb} \quad \text{and}$$
$$D_P = -\sum_{nb=n,w,e,s} D_{nb}.$$

As presented in the main text, there are two iterative procedures in the algorithm. In the inner loop, we solve the nonlinear system by coupling the momentum, energy and species balance equations. In the outer loop, we iterate on the time step. Let k and n denote the inner and outer loops, respectively. By using the backward-Euler scheme to discretized the time operator in semi-discretized Eq. (A.3), the spatial and temporal discretized form of Eq. (A.3) at the current inner-loop step $k+1$ and the current time step $n+1$ is written as

$$a_{o,P}^{n+1,k} H_{o,P}^{n+1,k+1} + a_{s,P}^{n+1,k} H_{s,P}^{n+1,k+1} - b_P^n = \sum_{nb} F_{nb}^{n+1,k} H_{o,nb}^{n+1,k+1} + \sum_{nb} D_{nb}^{n+1,k} T_{nb}^{n+1,k+1}, \tag{A.4}$$

where, $a_{j,P} = \Delta z \Delta r / \Delta t (S_j c_j)_P; j = o, s$, and $b_P^n = \Delta z \Delta r / \Delta t \left(\sum_{j=o,s} S_j c_j H_j\right)_P^n$. The unknowns in Eq. (A.4) are the temperature and enthalpy variables. The coefficients $F_{nb}^{n+1,k}$, $D_{nb}^{n+1,k}$, $a_{o,P}^{n+1,k}$, $a_{s,P}^{n+1,k}$, and b_P^n are calculated from previous iterations. For the sake of clarity, we drop the indicators k and n and define the function G_P in terms of the temperature and enthalpy variables:

$$G_P(T) \equiv a_{o,P} H_{o,P} + a_{s,P} H_{s,P} - \sum_{nb} F_{nb} H_{nb} - \sum_{nb} D_{nb} T_{nb} - b_P = 0. \tag{A.5}$$

References

[1] D. Shock, J.D. Sudburg, J.J. Crockett, Studies of the mechanism of paraffin deposition and its control, J. Pet. Tech. 7 (9) (1955) 23–30.
[2] R.M. Jorda, Paraffin deposition and prevention in oil wells, J. Pet. Tech. 237 (1966) 1605–1612.
[3] C. Narvaez, A.A. Ferrer, S.A. Corpoven, Prevention of paraffin well plugging by plunger-lift use, SPE 21640 presented at the SPE production operation symposium, Oklahoma City, Oklahoma, 7–9 April, 1991.
[4] J. Svetgoff, Paraffin problems can be resolved with chemicals, Oil Gas J. 82 (9) (1984) 79–82.
[5] B.J. Eastund, K.J. Schmitt, D.L. Meek, D.C. Anderson, G. Grisham, New system stops paraffin buildup, Pet. Eng. Int. 61 (1) (1989) 46–51.
[6] C. Lira-Galeana, A. Firoozabadi, J.M. Prausnitz, Thermodynamics of wax precipitation in petroleum mixtures, AIChE J. 42 (1) (1996) 239–248.
[7] P.A. Bern, V.R. Withers, J.R. Cairns, Wax deposition in crude oil pipelines, Proc. Euro. Offshore Petro. Conf. Exhib. Paper EUR 206. October 21–24, London, England, 1980.
[8] E.D. Burger, T.K. Perkins, J.H. Striegler, Studies of wax deposition in the Trans-Alaska Pipeline, J. Pet. Tech. 33 (6) (1981) 1075–1086.
[9] A. Majeed, B. Bringedal, S. Overa, Model calculates wax deposition for N. Sea oils, Oil Gas J. 88 (25) (1990) 63–69.
[10] T.S. Brown, V.G. Niesen, D.D. Erickson, Measurement and prediction of the kinetics of paraffin deposition, J. Pet. Tech. 47 (4) (1995) 328–329.
[11] J.A. Svendsen, Mathematical modeling of wax deposition in oil pipeline systems, AIChE J. 39 (8) (1993) 1377–1388.
[12] A.A. Hamouda, J.M. Ravnoy, Prediction of wax deposition in pipelines and field experience on the influence of wax on drag-reducer performance, in: Offshore Tech. Conf., OTC 7060 24th Annual OTC in Houston, Texas, May 4–7, 1992.
[13] F.S. Ribero, P.R.S. Mends, S.L. Braga, Obstruction of pipelines due to paraffin deposition during the flow of the crude oil, Int. J. Heat Mass Transfer 40 (18) (1997) 4319–4328.
[14] J.L. Creek, B. Matzain, M. Apte, M. Volk, E. Delle Case, H. Lund, Mechanisms for wax deposition, AIChE Spring National Meeting, Houston, TX, March 1999.
[15] P. Singh, H.S. Fogler, R. Venkatsean, N. Nagarajan, Formation and aging of incipient thin film wax–oil gels, AIChE J. 46 (5) (2000) 1059–1074.

[16] E. Ramirez-Jaramillo, C. Lira-Galeana, O. Manero, Modeling wax deposition in pipelines, Petroleum Sci. Technol. 22 (7–8) (2004) 821–861.
[17] M. Lacroix, V.R. Voller, Finite difference solutions of solidification phase change problems: transformed versus fixed grids, Numer. Heat Mass Transfer Part B Fundamentals 17 (1) (1990) 25–41.
[18] A.D. Brent, V.R. Voller, K.J. Reid, Enthalpy porosity technique for modeling convection–diffusion phase-change: application to the melting of pure metal, Numer. Heat Transfer 13 (3) (1988) 297–318.
[19] K. Fukui, K. Meada, Numerical simulation of dynamic layer solidification for a eutectic binary system, J. Chem. Eng. Jpn. 31 (3) (1998) 445–450.
[20] M. Mbaye, E. Bilgen, Phase change process by natural convection–diffusion in rectangular enclosures, Heat Mass Transfer 37 (1) (2001) 35–42.
[21] V.R. Voller, C. Prakash, A fixed grid numerical modeling methodology for convection–diffusion mushy region phase-change problems, J. Heat Mass Transfer 30 (18) (1987) 1709–1719.
[22] C.H.S. Lira, Solidification in square section, Theoria 10 (2001) 47–56.
[23] G.A. Holder, J. Winkler, Wax crystallization from distillate fuels: I. cloud and pour phenomena exhibited by solutions of binary *n*-paraffin mixtures, J. Inst. Petrol. 51 (499) (1965) 228–235.
[24] G.A. Holder, J. Winkler, Wax crystallization from distillate fuels. Part II: mechanisms of pour depression, J. Inst. Petrol. 51 (499) (1965) 235–243.
[25] A.A. Hamouda, S. Davidsen, An approach for simulation of paraffin deposition in pipelines as a function of flow characteristics with reference to Tesside oil pipeline, in: SPE 28966-MS, Proc. SPE Int. Symp. on Oilfield Chemistry, San Antonio, TX, February 14–17, 1995.
[26] G.M. Elphingston, K.L. Greenhill, J.J.C. Hsu, Modeling of multiphase wax deposition, J. Energy Res. Tech. 121 (2) (1999) 81–85.
[27] P. Singh, H.S. Fogler, R. Venkatesan, Morphological evolution of thick wax deposits during aging, AIChE J. 47 (1) (2001) 6–18.
[28] W.M. Deen, Analysis of Transport Phenomena, Oxford University Press, New York, 1998.
[29] D.E. Rosner, Transport Processes in Chemically Reacting Flow Systems, Courier Dover Publications, 2000.
[30] P.C. Carman, Fluid flow through granular beds, Trans. Inst. Chem. Eng. 15a (1937) 150–166.
[31] R.B. Bird, W.E. Stewart, E.N. Lightfoot, Transport Phenomena, second ed., John Wiley, 2002.
[32] H. Hoteit, R. Banki, A. Firoozabadi, Deposition and aging in flow lines from irreversible thermodynamics, submitted for publication.
[33] H.S. Carslaw, J.C. Jaeger, Conduction of Heat in Solids, second ed., Oxford University Press, New York, 1959.
[34] S. Whitaker, The Method of Volume Averaging, Kluwer Academic, Springer, Boston, 1999.
[35] A. Firoozabadi, Thermodynamics of Hydrocarbon Reservoirs, McGraw-Hill, New York, 1999.
[36] C.A. Passut, R.P. Danner, Heat capacity and entropy, Ind. Eng. Chem. Process Des. Develop. 11 (4) (1972) 543.
[37] P. Singh, H.S. Fogler, N. Nagarajan, Prediction of the wax content of the incipient wax–oil gel in a flowloop: An application of the controlled-stress rheometer, J. Rheol. 43 (6) (1999) 1437–1459.
[38] K. Ghorayeb, A. Firoozabadi, Molecular pressure and thermal diffusion in nonideal multicomponent mixtures, AIChE J. 46 (5) (2000) 883–891.
[39] A. Firoozabadi, K. Ghorayeb, K. Shukla, Theoretical model of thermal diffusion factors in multicomponent mixtures, AIChE J. 46 (5) (2000) 892–900.
[40] A. Leahy-Dios, M.M. Bou-Ali, J.K. Platten, A. Firoozabadi, Measurements of molecular and thermal diffusion coefficients in ternary mixtures, J. Chem. Phys. 122 (23) (2005) 1–12.
[41] D. Nichita, L. Goual, A. Firoozabadi, Wax precipitation in gas condensate systems, SPE Prod. Facilit. 16 (4) (2001) 250–259.
[42] R.A. Heidemann, J. Madsen, E.H. Stenby, S.I. Andersen, Wax precipitation modeled with many mixed solid phases, AIChE J. 51 (1) (2005) 298–308.
[43] S.V. Patankar, Numerical Heat Transfer and Fluid Flow, Hemisphere Publishing Corp., Washington, 1980.
[44] H.K. Versteeg, W. Malalasekera, An Introduction to Computational Fluid Dynamics, Pearson Prentice Hall, Essex, England, 1995.
[45] J. Lohrentz, B. Bray, R. Clark, Calculating viscosities of reservoir fluids from their compositions, J. Pet. Tech. 16 (1964) 1171–1176.